Earth`s Cryosphere, 2019, vol. XXIII, No. 3, pp. 43–50 **http://earthcryosphere.ru/**

DOI: 10.21782/EC2541-9994-2019-3(43-50)

ICE RIDGES IN THE SHOKALSKY STRAIT, THE SEVERNAYA ZEMLYA ARCHIPELAGO

V.V. Kharitonov

Arctic and Antarctic Research Institute,
38, Beringa str., St. Petersburg, 199397, Russia; sogra.kharitonov@mail.ru

The paper discusses the main characteristics of the three first-year ice ridges examined with respect to their geometry and morphology in the Shokalsky Strait (Severnaya Zemlya Archipelago) in April and May 2016. These studies were conducted using hot water thermal drilling with computer-recording of penetration rate. The boreholes drilled along the transect of the top of the ridge were spaced at 0.25 m. Cross-sectional profiles of the ice ridges are presented. The measured dimensions of the studied ice ridges were: sail height varying from 2.5 up to 3.4 m, the keel depth varying from 8.3 up to 10.3 m. The keel depth to sail height ratio averaged from 2.8 to 3.3 m, and the thickness of the consolidated layer was 2.2–2.4 m. The porosity of the unconsolidated part of the keel was about 25–30 % in two ridges and about 19 % in the third one. The distributions of volume content of solid phase in sea ice versus depth are analysed for all the studied ice ridges. One of these ice ridges was characterized by an extremely steep keel slope angle (about 87°).

Ice ridge, thermal drilling, cross-sectional profile, consolidated layer, keel slope

INTRODUCTION

Unlike morphometric studies of undeformed ice, the studies related to morphometric features of ice ridges inherent in extensive areas of sea ice cover do not have a rich history, while amount of observations available today is by all accounts plainly scant. L. Strub-Klein and D. Sudom [*2012*] have made a review of long-term studies of sea ice ridges in Arctic seas and analyzed the best available data since 1971, accumulated by foreign and Russian researchers. Some of the existing knowledge gaps have been successfully bridged by D. Sudom and G. Timco in [*Sudom and Timco, 2013*]. Sea ice ridges are fairly exhaustively studied in the freezing water areas on Russian seas shelves, inasmuch as their morphometric characteristics, primarily the thickness of consolidated layer (CL)* are critical at the design stage for assessment of loads acting on offshore structures. Despite the fact that the data have recently been updated (e.g. [*Pavlov et al., 2016*]), very few attempts have been made to investigate morphometry of deformed ice and sea ice ridges in the Laptev and East Siberian seas, and, in particular, such information is simply unavailable for the Shokalsky Strait. Due to the climate change-driven drastic reduction in Arctic sea ice area and its thickness, this actually provides one of the major challenges, and therefore any new findings about the internal structure of modern ice ridges would be of great practical value. Our research contributes to this problem solution by filling existing gaps with new data on ice ridges obtained in the study area. Tackling this problem involved the following tasks:

– selecting most illustrative objects of study;

– analysis of morphometric characteristics and internal structure of sea ice ridges;

– obtaining information about consolidated layer thickness and variation within the ridge.

Recent works on this subject are fairly numerous [*Strub-Klein et al., 2009; Strub-Klein and Høyland, 2011; Sand et al., 2013*], which primarily analyze results morphometric studies of ice ridges in the Barents sea and in the Fram Strait. The morphometric characteristics also include comparison of first- and second-year ridges. It should be mentioned that the keel of second-year ice ridges is almost completely consolidated, and the morphometric characteristics of the studied ridges are mainly typical of the ridges in the Barents sea. Much attention is paid to the ocean currents impacts on the keel erosion. Small ridges in the landfast ice are more susceptible to keel erosion than larger ice ridges. Noteworthy is that in May solar radiation invokes a decrease in the thickness of ice blocks in the sail. A contribution of new data on the parameters of ridges is eccentiated in [*Sand et al., 2015*], which were found to be insufficient according to [*Sudom and Timco, 2013*]. These parameters include: keel width, slope angles of the sail and keel, the area occupied by the keel on the cross-section of the ridge, the CL thickness. Remarkably persisting is the lack of resources required for con-

* Consolidated layer of ice ridge is a layer of dense (solid) ice with the upper boundary approaching waterline, which forms as a result of the action of cold and freezing of water between randomly oriented rubble blocks with these blocks included in its structure, while its strength is nearly equal to the strength of the level ice.

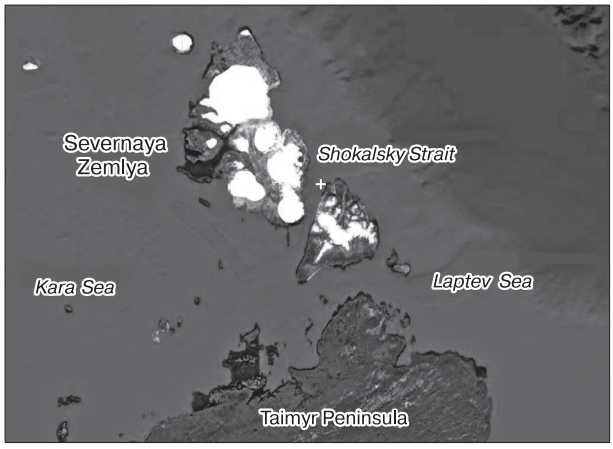

Fig. 1. Location map of the area of works.
Location of the test site is marked by "+".

ducting comprehensive ice investigations. The ridges in the Russian sector of the Barents sea were studied by A.K. Naumov [*2010*], who has provided valuable insights into the ridge sails and keels geometry in the eastern Barents and inferred that ridge shapes and geometries are fairly on par with the values obtained for the Bering, Baltic and Labrador seas, however, differing significantly from the values for the Arctic basin and the Beaufort sea.

The morphometric characteristics of ridges in the Caspian sea are discussed in [*Mironov and Porubaev, 2011*] and those in the Kara sea are analyzed in [*Mironov and Porubaev, 2012*]. Maximum values of the keel depth of the ridges in the Caspian sea reach 7 m. The average height of sails of ridges in the Kara sea is 3.2 m, at average keel depth of 11.5 m, with their values peaking at 4.5 m and 15.7 m, respectively. The research results presented in [*Shestov and Marchenko, 2014*] are concerned with the ridge keels and sea currents inside the ridge keel, as well as in the vicinity of ice ridge under level ice. The sea currents inside the unconsolidated part of the keel fill the voids with water, while their speed is 3 times higher than the speed of sea currents under the surrounding level ice. M. Suominen and colleagues obtained the morphological characteristics of ridges by drilling and then compared them with the sonar data [*Suominen et al., 2017*]. In this experiment, very small ridges were selected, to let the ship pass through them at the first attempt. Therefore, the maximum depth of the keel of such ridges was only 5 m.

This article provides morphometric characteristics and features of internal structure of three ice ridges investigated using hot-water drilling in the spring of 2016 in the area of landfast ice on the Shokalsky Strait, the Severnaya Zemlya archipelago (Fig. 1). The team of researchers was based at the Ice Base Cape Baranova research station owned by the Arctic and Antarctic Research Institute, AARI.

Most of the landfast ice adjoining the research station to ridged ice with sail heights not exceeding 1.0–1.5 m. At a distance of 5 km from the base we found three ice ridges with the height of the sail more than 2 m, which were chosen as study objects. The set up test site encompassed all three ice ridges, as well as surrounding level and rafted ice. The thickness of the level ice varied between 1 and 2 m. The ridges were located approximately on the same line spaced at 570 and 700 m from each other.

ICE RIDGE RESEARCH METHODS

The internal structure of ridges was studied using the UVBL-2 hot-water drilling (HWD) system manufactured by AARI, including water heater, hot-water drill and data logger to record the rates of penetration. This technology is ranked as unique, given that auger drilling with manual record keeping of encountered ice areas with different porosity and voids is dominantly applicable abroad. The drill system was powered by a 4 kW gasoline generator (see Fig. 2 for

Fig. 2. Overview of the UVBL-2 thermal (hot-water) drilling system for ice drilling.
The figure shows deployed operations of two HWD posts. The 2016 drilling works involved only one post.

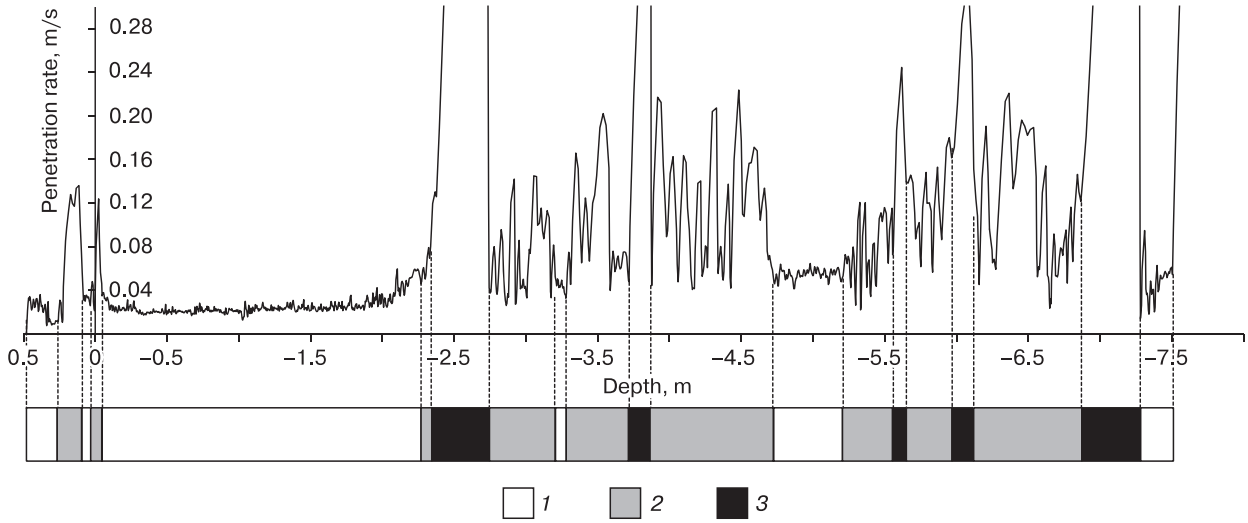

Fig. 3. An example of the ice ridge drilling rates record and revealed locations of ice segments with different porosity along the drilled hole inferred from the resulting diagram.

1 – hard ice; *2* – porous ice; *3* – void.

its general view). Seawater is pumped by electric pumps through the mixing pipe and suction hose and passes through the water heater, where it is heated by a boiler running on diesel fuel. Some of the hot water is drained into the mixing pipe to heat the water sucked into the heater. Water heated to a temperature of 80–90 °C, comes to the measuring boxes via inlet hoses wound on reels. During the operations, as the distance from the drilling systems grows, the supply hoses become unwound and stretch on the ice surface. The measurement include: drill displacement transducer (LIR angle sensor), water temperature sensor, and logger. Hot water is then pumped and pressurized through the drill hose to hot water drills. While drilling, the drill hose rotates the measuring wheel of the transducer. The penetration rate was calculated using the calibration coefficients previously determined in laboratory conditions. Drilling was carried out along the profiles laid across the tops of the ridges. An example of penetration rate record is shown in Fig. 3. The average rate of hot-water drilling (HWD) of dense ice is 0.02–0.04 m/s.

Morphometric characteristics of the ridges and their internal structure were derived from the thermal drilling data processing [*Morev et al., 2000*]. The drilling rate is cumulatively governed by heat power supplied to the hot-water drill, the porosity of ice and to much lesser extent by its temperature. Locations of voids, hard and porous ice on borehole sections are largely prompted by the penetration. A necessary condition for validity of this definition would be either drilling of holes at a constant heat power or monitored changes in heat power while drilling. In regions of porous ice, specifically, with voids filled with snow, sludge, water or air, the thermal drill movement is strongly accelerated. Additionally, the distance between the snow (ice) surface to sea level is constantly measured. The thermal drilling data processing involved determinations of the values of surface and underwater parts of the sea ice cover, as well as CL boundaries of ridges, voids contacts, areas of ice with different porosity.

Ice ridge 1 was transected by 8 profiles across its top, along which 0.25 m-spaced holes were drilled. At the line edges, where the ice ridge consolidation reached 100 %, the spacing was larger, 0.5–1 m. In the central part of the ridge, the distance between lines reached 2 m. One transect was laid across each of the Ice ridges numbered 2 and 3. The snow cover depth and ice surface above sea level were measured at each measurement point. A visual inspection of the lower surface of the ridges using TPA Gnom, a remote-controlled underwater vehicle (RCUV) and sonar was also performed.

DICSUSSION OF RESULTS

During the period from April 11 through May 28, 2016, three ice ridges were studied in detail. Their main morphometric characteristics are given in Table 1. Figure 4 shows the profiles of the studied ridges. Mean sail block thickness (Ice ridge 1 and 2) was about 0.28 m, ice ridge measured 3 – 0.36 m. At the drilling site, the sail of Ice ridge 3 was buried under a thick layer of snow, with the snow cover depth (SCD) locally exceeding 2 m.

All the studied ridges have their own distinctive features. The first ridge is characterized by an extremely large angle of the keel slope, averaging 87°.

Table 1. **Morphometric characteristics of sea ice ridges**

Characteristics	Ridge 1	Ridge 2	Ridge 3
Number of transects (profiles) through ridge cross-section	8	1	1
Number of holes drilled	885	123	105
Mean/max ice thickness, m	5.06/13.26	5.34/10.44	4.39/9.58
Mean max sail height, m	1.59/3.44	1.57/2.54	1.09/2.97
Mean/max keel depth, m	4.84/10.27	4.97/8.33	4.36/8.32
Mean value of upper boundary of CL*, m	0.06	–0.08	–0.01
Mean value of lower boundary of CL, m	–2.34	–2.26	–2.26
Mean CL thickness, m	2.40	2.16	2.25
Min/mean/max surrounding level ice thickness, m	0.93/1.40/1.61	1.36/1.69/1.93	1.50/1.65/1.87
Sail angles, degr.	24.2–77.5	25.4–38.1	20.3–46.8
Keel angles, degr.	11.2–87.5	24.0–64.3	22.8–40.9
Mean ridge porosity**	0.13	0.11	0.15
Mean sail porosity	0.24	0.13	0.22
Mean keel porosity	0.14	0.11	0.15
Mean porosity in nonconsolidated part of ridge	0.28	0.25	0.30
Max keel/max sail	3.0	3.3	2.8
Mean CL thickness/mean ridge thickness	0.47	0.49	0.51
Mean CL thickness/mean level ice thickness	1.71	1.28	1.36
Min/mean/max snow cover depth, m	0/0.19/1.97	0.05/0.38/1.11	0/0.81/2.15

*Consolidated layer.
**Linear porosity is the sum of voids length to drilled hole length ratio.

On one of the transects (profiles), this angle even takes a negative value (Fig. 4, *a*). It has been suggested that during the formation of the ice ridge the ice blocks formed a neat pile and progressively melted in addition, to form a nearly vertical wall. However, the visual inspection of the left slope of the keel of Ice ridge 1 showed the presence of randomly piled blocks. This phenomenon may occur in the process of MY ridging (formation of secondary ridge), when, for example, a partially consolidated keel of the ridge af-

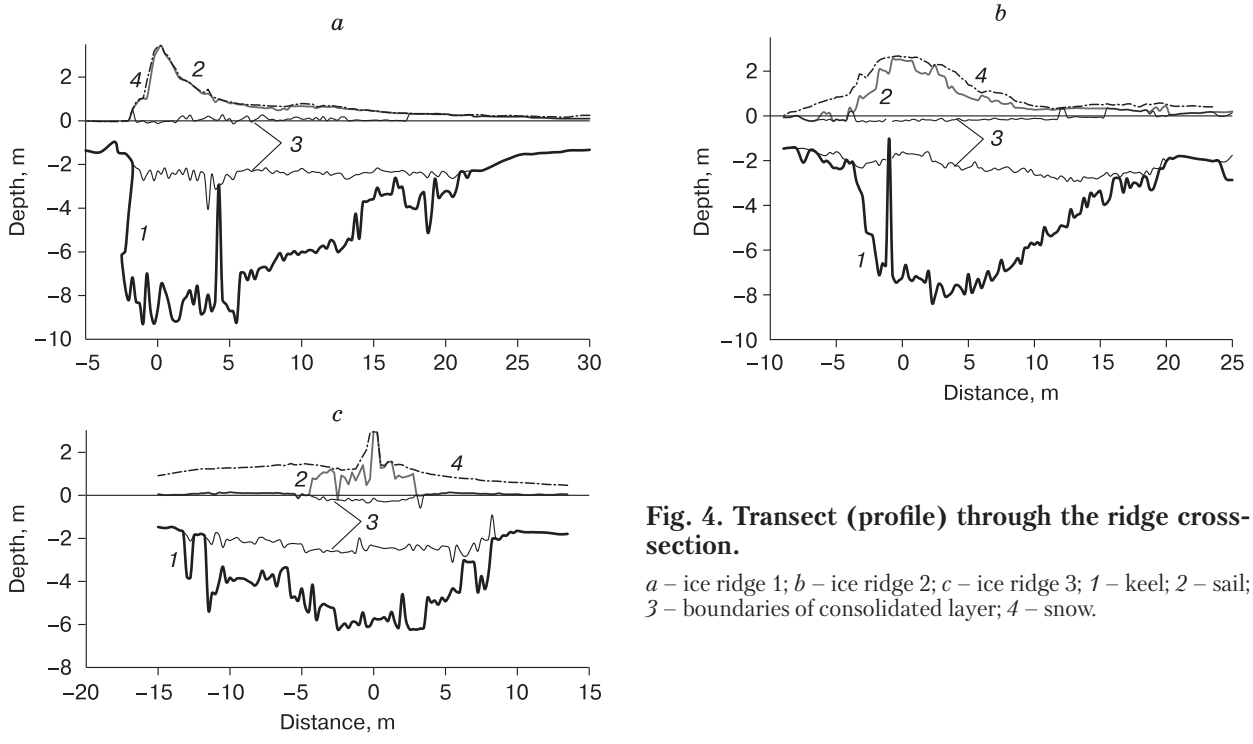

Fig. 4. Transect (profile) through the ridge cross-section.

a – ice ridge 1; *b* – ice ridge 2; *c* – ice ridge 3; *1* – keel; *2* – sail; *3* – boundaries of consolidated layer; *4* – snow.

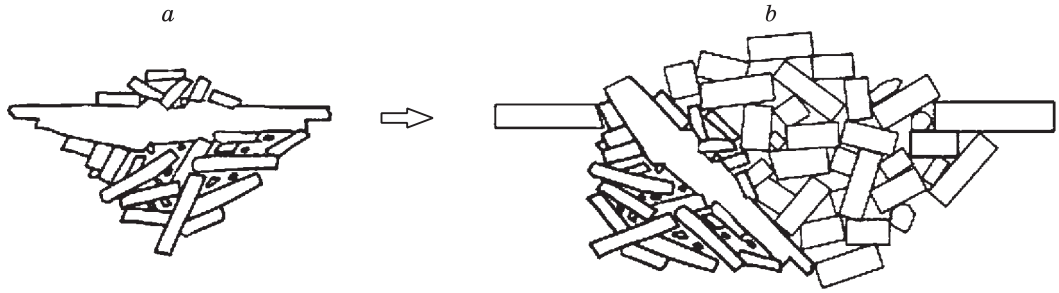

Fig. 5. One of the possible schemes of secondary (MY) ice ridge formation.

a – first-year (FY) ice ridge; *b* – multi-year (MY) ice ridge formation. The left slope of keel form a vertical wall.

fected by ice piling on its edge is submerging and rotating, then the slope of the keel can appear to be vertical. Figure 5 illustrates one of the possible schemes for MY ridging, when the FY (primary) ice ridge (Fig. 5, *a*) experiences compression as blocks of ice on its edge start piling up, thereby melting in addition the FY ice ridge and making it turn around the center (Fig. 5, *b*). Given a sufficiently large rotation angle of FY ice, ice blocks composing the lower part of its keel, a vertical wall can form within MY ridge on the keel edge of MY ridge. This undoubtedly requires careful and thorough consideration, but we can confidently ascertain the defection of a rare case of such formation of the ice ridge keel. The only similar example was offered by P. Kankaanpää [*1989*], however in that case, the drilling profile passed along the ridge. Table 2 lists the maximum values of the keel slope angle provided in various published sources.

Much attention has recently been paid by researchers to the little explored, but intriguing issue of CL thickness distribution inside the ridge. The information provided herewith can in part be used for this problem solution. The CL thickness of Ice ridge 1 was 2.4 m (mean), 4.3 m (max), 1.1 m (min). The consolidated layer is well developed and non-uniform in thickness. Unlike Ice ridge 1, the CL thickness of Ice ridge 2 varies in the range from 1.3 to 3.1 m, with the CL having a flat shape without abrupt changes in thickness, while thickness tends to be less under the sail, which may be dictated by the shielding effect of the sail, which precludes the penetration of cold to the ice ridge keel. The CL of Ice ridge 3 is slightly less in thickness (1.0–3.2 m) than in the case of the Ice ridges 1 and 2, probably due to younger age of Ice ridge 3, whose CL has pronouncedly bent down under the sail. For comparison, the data on consolidated layer available from the publications are listed in Table 2.

The CL thickness does not correlate with porosity of the unconsolidated part of the keel, however, there is a slight significant inverse correlation with the snow cover and ice above sea level (correlation coefficient –0.35). Thus, it can be stated that the CL of the studied ice ridges was determined not only by the density of rubble ice packing the keel, but in a greater extent by the access of cold to the unconsolidated keel. In most cases, the CL thickness tends to be thinner in the keel portion topped by the sail or a thick snow cover.

On ice ridge 1 in the right part of the keel, the CL thickness gradually decreases as the CL grades into level ice. The nature of this reduction is well approximated by the exponential function of the form

$$A + B \exp\left(1 + \frac{x}{x_0}\right)^3.$$

According to the energy conservation law, a relationship between the thermal drilling rate and the power can be expressed by the calorimetric formula

$$v = KP \Big/ \Big[\Lambda\big(\rho(1-a-s)\big(-c_i t_i + L\big) - \\ -\rho_w s c_w t_i + \big(\rho(1-a-s) + \rho_w s\big) c_w t_w \big)\Big], \quad (1)$$

where v is penetration rate of hot water drill, m/s; P is thermal power going to hot water drill, W; K is coefficient factoring in heat dissipation through the side wall of hot water drill bit (drill bit performance); Λ is frontal area of hot water drill bit, m^2; ρ is monocrystal

Table 2. **Some morphometric characteristics of ice ridges from published literature**

α_{max}, degr.	h_{CL}, m	h_{CL}/h_i	Source
32	–	–	[*Weeks et al., 1971*]
52*	–	–	[*Grishchenko, 1988*]
64	–	–	[*Kankaanpää, 1989*]
80–90	–	–	[*Timco and Burden, 1997*]
29	1.9	1.3–1.6	[*Bonnemaire et al., 2003*]
–	1.5–2.2	–	[*Mironov and Porubaev, 2005*]
78	1.8–5.4	1.1–3.5	[*Kharitonov, 2012*]
58	0.4–3.0	1.3–1.6	[*Kharitonov, 2013*]
35	1.5–1.9	1.9–2.0	[*Sand et al., 2013*]
29	1.2–1.8	1.9–2.5	[*Sand et al., 2015*]

Note. α_{max} is maximal keel angle; h_{CL} is average consolidated layer (CL) thickness; h_{CL}/h_i is the average CL thickness to average level ice thickness ratio.

*For thin-ice (<0.3 m) ridges.

ice density, kg/m^3; a is volume air content in ice; s is volumetric brine content in ice; c_i is pure ice heat capacity, J/(kg·°C); t_i is ice temperature, °C; L is heat of ice melting, J/kg; ρ_w is melt mass density, kg/m^3; c_w is heat capacity of melt mass, J/(kg·°C); t_w is temperature of melt mass, °C. We define volume content of ice solid phase, *VCI* (volume content of ice), as

$$VCI = 1 - a - s. \quad (2)$$

The *VCI* value is equal to one less porosity and is identical with the filling factor, being however slightly lower given that it takes into account the presence of micropores in ice blocks.

Then from (1) and (2) the penetration rate v inversely proportional to the volume content of ice solid phase:

$$VCI \approx \frac{K(VCI)P}{\Lambda\rho L} \cdot \frac{1}{v}. \quad (3)$$

The expression K (*VCI*) signify that, strictly speaking, the coefficient K can depend on the volume content of ice solid phase (*VCI*). The nature of this dependence is unknown and difficult to determine. However, due to a high penetrating rate of hot-water drill bit, the volume content of ice solid phase (*VCI*) effect on the drill bit performance, i.e. on the constant K, will be leveled off.

Thus, as a first approximation it can be assumed that the constant of proportionality between the penetrating rate v and volume content of ice solid phase (*VCI*) in (3) does not depend on the volume content.

The depth-dependent inverse rate (velocity) value is the distribution of the volume content of ice solid phase along the borehole expressed in relative units, inasmuch as the constant of proportionality has the dimension of velocity. The exact *VCI* values are undefinable because the constant of proportionality between *VCI* and inverse velocity is unknown. Thus, for simplicity, the values of $1/v$ are used as some relative *VCI* values. This distribution will therefore be individual for each well. Averaging these curves over all wells allows to obtain an average distribution of the volume content of the solid ice phase with depth for a discrete ridge or for the entire study area. The averaging procedure is discussed below.

All the depths are considered successively: from the maximum sail height to the minimum keel depth. At each chosen depth, the $1/v$ values are averaged over all boreholes corresponding to this depth. In boreholes where the considered depth is determined beyond the sail or keel, the value of $1/v$ is assumed to be zero.

Figure 6 shows the distribution of volume content of ice solid phase with depth for the studied ridges. The consolidated layer is distinguished by a sharp increase in the volume content of solid ice phase near the waterline. The longer the ridge was exposed to cold, the greater the thickness of its CL and the smaller the variation of its lower boundary positions.

This is reflected in the *VCI* curve behavior within the depth range from –1 to –2.5...–3 m. The curve is tending to be flatter. The ridges were studied during the time spans, each successively approaching summer: April, 14–16 (Ice ridge 1); May 8–11 (Ice ridge 2); May 24–25 (Ice ridge 3). The implications are that the ice of the ridges was progressively warm-

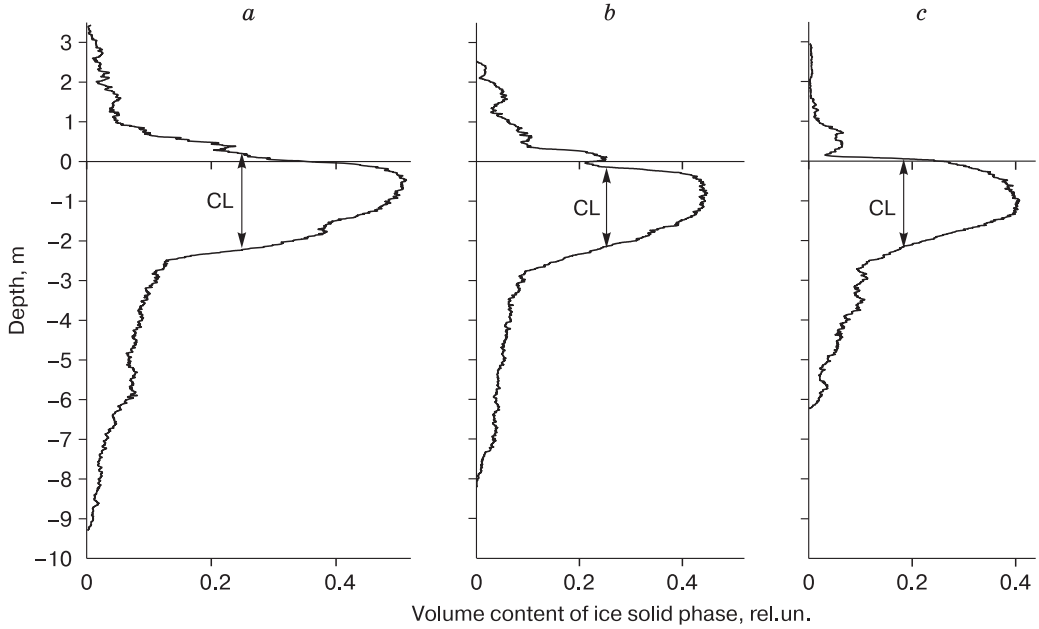

Fig. 6. Distribution of volume content of ice solid phase through depth for the studied ice ridges.

a – ice ridge 1; *b* – ice ridge 2; *c* – ice ridge 3. CL – consolidated layer.

ing, the average penetration rate increased, which was reflected in the records, accordingly. Thus the CL parameters were distributed among the studies ridges as follows: *VCI* = 0.5, v = 2 cm/s (Ice ridge 1), *VCI* = 0.43, $v \approx 2.3$ cm/s (Ice ridge 2), *VCI* = 0.4, v = 2.5 cm/s (Ice ridge 3).

The top plateau of the *VCI* curve for Ice ridge 2 in the 0.3...–0.3 m depth interval shown in Fig. 6, *b* is actually divided into two parts, which results from the formation of ice rafted while ridging and subsequent consolidation at the distance of 15.5–19 m (Fig. 4, *b*). The CL of the ridge exhibits a sharp thickening showing such a gap on the upper CL boundary distribution.

The *VCI* curve shown in Fig. 6, *c* decreases sharply in the depth range 0...–0.6 m. As such, the *VCI* distribution, corresponding to the upper CL boundary, was largely due to the fact that Ice ridge 3 was studied during the period of May 24–25 when solar radiation-induced thermal degradation of the upper layer of CL had already begun.

CONCLUSIONS

The conducted research allowed to obtain new data on sea ice cover on the Shokalsky Strait. The results analysis allowed the following inferences:

– max keel/max sail for the studied ridges is equal to 3.2, 3.3, and 2.8, respectively;

– the CL thickness in these ridges varied from 1.0 to 4.3 m, with CL thickness averaging 2.2–2.4 m; the CL thickness was determined by rubble ice mass density in the keel (to a lesser extent) and by cold penetration in the unconsolidated keel (to a greater extent);

– mean CL thickness/mean level ice thickness ratios for the studied ridges (1, 2 and 3) are 1.71, 1.28 and 1.36;

– the consolidation degree of all ridges was approximately 50 %;

– at the edges of ice ridge where the ridge is fully consolidated, the CL gradually decreases and grades into the level ice, while the CL thickness changes exponentially;

– the reported maximum keel slope angle of Ice ridge 1 is about 87°, on average, which have reached negative values in certain areas of the ice ridge keel.

The author thanks the AARI staff and in person R.A. Savin and G.A. Deshevykh for their help in thermal drilling of ice ridges.

References

Bonnemaire, B., Høyland, K.V., Liferov, P., Moslet, P.O., 2003. An ice ridge in the Barents Sea, part I: morphology and physical parameters in-situ. In: Proc. of the 17th Intern. Conf. on Port and Ocean Engineering under Arctic Conditions, Trondheim, Norway, June 16–19, 2003.

Grishchenko, V.D., 1988. Morphometric characteristics of ice ridges in the Arctic Basin. Proceeding of AARI, vol. 401, 46–55.

Kankaanpää, P., 1989. Structure of first-year ridges in the Baltic Sea. In: Proc. of the 10th Intern. Conf. on Port and Ocean Engineering under Arctic Condition, POAC'89, June 12–16, 1989, Luleå, Sweden, Luleå University of Technology, vol. 1, pp. 87–102.

Kharitonov, V.V., 2012. Internal structure and porosity of ice ridges investigated at "North Pole 38" drifting station. Cold Regions Science and Technology, vol. 82, 144–152.

Kharitonov, V.V., 2013. On the results of research of the internal structure of ice ridges in the "North Pole – 2010" expedition at Barneo ice camp in April 2010. In: Proc. of the 22nd Intern. Conference on Port and Ocean Engineering under Arctic Conditions (POAC), Espoo, Finland, June 9–13, 2013.

Mironov, Ye.U., Porubaev, V.S., 2005. Structural peculiarities of ice features of the offshore of the Caspian Sea, the Sea of Okhotsk and the Pechora Sea. In: Proc. of the 18th Intern. Conf. on Port and Ocean Engineeging under Arctic Conditions (POAC), Potsdam, New York, June 26–30, vol. 2, pp. 483–492.

Mironov, Ye.U., Porubaev V.S., 2011. Morphometric parameters of ice ridges and stamukhas from the data of expeditionary research in the Northwestern Part of the Caspian Sea. Russian Meteorology and Hydrology, No. 5, 68–76.

Mironov, Ye.U., Porubaev, V.S., 2012. Formation of ice ridges in the coastal part of the Kara sea and their morphometric characteristics. Modern Problems of Science and Education, No. 4. – URL: http://science-education.ru/ru/article/view?id=6707 (submittal date: 05.07.2018).

Morev, V.A., Morev, A.V., Kharitonov, V.V., 2000. Method of determination of ice ridge and stamukha structure, ice features and boundaries of ice and ground. Patent RU 2153070 C1. Russian Federation: MPK E21C 39/00 (2000.01), G01N 9/00 (2000.01). Patent Holders: authors. – No. 2153070. Claimed 19.11.1998. Published 20.07.2000, Bull. No. 20. (in Russian)

Naumov, A.K., 2010. Morphometric characteristics of ice formations of the Barents sea. Abstract of the PhD thesis. St. Petersburg, 12 pp. (in Russian)

Pavlov, V.A., Kornishin, K.A., Efimov, Ya.O., Mironov, E.U., et al., 2016. Peculiarities of consolidated layer growth of the Kara and Laptev Sea ice ridges. Neftyanoe Khozyaystvo (Oil Industry), No. 11, 49–54.

Sand, B., Petrich, C., Sudom, D., 2013. Morphologies of ridges surveyed off Svalbard and in Fram Strait, 2011 and 2012 field expeditions. In: Proc. of the 22nd Intern. Conf. on Port and Ocean Engineering under Arctic Conditions (POAC), Espoo, Finland, June 9–13, 2013.

Sand, B., Bonath, V., Sudom, D., Petrich, C., 2015. Three years of measurements of first year ridges in the Barents Sea and Fram Strait. In: Proc. of the 23th Intern. Conf. on Port and Ocean Engineering under Arctic Conditions (POAC), Trondheim, Norway, June 14–18, 2015.

Shestov, A.S., Marchenko, A.V., 2014. Properties of ice ridge keels and sea currents in their vicinity in the Barents Sea. In: Proc. of the 22th IAHR Intern. Symp. on Ice, Singapore, August 11–15, 2014.

Strub-Klein, L., Barrault, S., Goodwin, H., Gerland, S., 2009. Physical properties and comparison of first- and second-year sea ice ridges. In: Proc. of the 20th Intern. Conf. on Port and Ocean Engineering under Arctic Conditions, Luleå, Sweden, June 9–12, 2009.

Strub-Klein, L., Høyland, K., 2011. One season of a 1st year sea ice ridge investigation – Winter 2009. In: Proc. of the 21st Intern. Conf. on Port and Ocean Engineering under Arctic Conditions, Montréal, Canada, July 10–14, 2011.

Strub-Klein, L., Sudom, D. A., 2012. comprehensive analysis of the morphology of first-year sea ice ridges. Cold Regions Science and Technology, vol. 82, 94–109.

Sudom, D., Timco, G., 2013. Knowledge gaps in sea ice ridge properties. In: Proc. of the 22nd Intern. Conf. on Port and Ocean Engineering under Arctic Conditions (POAC), Espoo, Finland, June 9–13, 2013.

Suominen, M., Polojärvi, A., Oikkonen, A., 2017. Ridge profile measurements for understanding ridge resistance. In: Proc. of the 24th Intern. Conf. on Port and Ocean Engineering under Arctic Conditions, Busan, Korea, June 11–16, 2017.

Timco, G.W., Burden, R.P., 1997. An analysis of the shapes of sea ice ridges. Cold Region Science and Technology, vol. 25, 65–77.

Weeks, W.F., Kovaks, A., Hibler III, W.D., 1971. Pressure ridge characteristics in the Arctic coastal environment. In: Proc. of the 7th Intern. Conf. on Port and Ocean Engineering under Arctic Condition, POAC'71, Trondheim, Norway, August 23–30, 1971, vol. 1, pp. 152–183.

Received April 2, 2018
Revised version received September 10, 2018
Accepted January 10, 2019